Optical Fiber Technology 30 (2016) 32–37

Contents lists available at ScienceDirect

Optical Fiber Technology

www.elsevier.com/locate/yofte

Regular Articles

Optical fiber Fabry–Perot interferometer for microorganism growth detection

Xiaohui Liu, Mingshun Jiang *, Qingmei Sui, Shuyang Luo, Xiangyi Geng

School of Control Science and Engineering, Shandong University, Jinan 250061, Shandong, China

ARTICLE INFO

Article history:
Received 17 June 2015
Revised 20 January 2016

Keywords:
Optical fiber sensor
Fabry–Perot interferometer
Hollow-core photonic crystal fiber
Microorganism growth detection

ABSTRACT

An optical fiber Fabry–Perot interferometer (FPI) based on hollow-core photonic crystal fiber (HCPCF) for microorganism growth detection is proposed and demonstrated. The FPI is formed by splicing both ends of a short section of HCPCF to SMFs and cleaving the SMF pigtail to a proper length. By measuring the fringe contrast of interference pattern, the refractive index (RI) changes of analyte during microorganism growth can be obtained. RI response of the sensor was investigated theoretically and experimentally. It shows linear response with sensitivity of −136 dB/RIU and good repeatability. Temperature response was also tested and the result confirms the low temperature cross-sensitivity of the sensor. Detection of yeast growth in liquid medium by the FPI sensor was conducted and the result shows the characteristic of typical yeast growth curve. With its advantages of high RI sensitivity, low temperature cross-sensitivity, capability for real-time measurement and so on, this FPI sensor has great potential in biosensing.

1. Introduction

Biosensors have been widely investigated over the past decades, and the detection of microorganism has been a hotspot for its significance in microbiology, medical diagnosis, food safety and environment monitoring. Optical fiber biosensors have attracted great attention recently due to many desirable advantages, such as small size, compact structure, high flexibility, immunity to electromagnetic interference, corrosion resistance, and the capability for in situ and multiplexed operation. Various optical fiber biosensors have been developed including tapered fiber [1], optical fiber surface plasmon resonance (SPR) device [2,3], fiber Bragg grating (FBG) [4,5], tilted fiber Bragg grating (TFBG) [6,7], long period grating (LPG) [8,9], fiber modal interferometer (MI) [10,11] and optical fiber Fabry–Perot interferometer (FPI) [12,13]. By measuring the changes of analyte refractive index (RI) or biofilm thickness that modulate the optical parameters, they can realize label-free biological detection with high sensitivity and fast response. However, tapered fiber sensors usually have weak strength; SPR sensors are relatively complicated to produce; for FBG biosensors some special processes such as chemical etching or side-polishing are required, thus the mechanical strength is reduced; TFBGs have limited detection accuracy due to their complex transmission resonance features; LPG biosensors typically exhibit high sensitivities but nonlinear responses and limited measurement range; and fiber MIs usually involve a long dimension undesirable for practical applications in biosensing. Moreover, most of them are cross-sensitive to temperature, so errors induced by temperature variations need to be compensated.

Optical fiber FPIs have extensive application prospect in biosensing owing to the advantages of compact probe structure, large measurement range, convenient reflection mode for signal detection, and suitability for in situ and remote measurement. All kinds of optical fiber FPI based biosensors have been proposed: extrinsic FPI [14] with open air cavity for analyte entering provides relatively high sensitivity, but the cavity is easily contaminated, lowering its measurement accuracy, and the extrinsic FPI formed by coating other materials [15,16] is sensitive to temperature; intrinsic FPI [17] with in-fiber reflecting mirrors is difficult to fabricate; inline FPI can be realized by femtosecond laser micromachining [18] or splicing different kinds of fibers, especially the inline FPI formed by photonic crystal fiber (PCF) and single mode fiber (SMF) [19,20] has the additional advantages of easy fabrication, low cost and low temperature cross-sensitivity.

In this paper, we propose an optical fiber FPI based biosensor fabricated by splicing both ends of a short section of hollow-core photonic crystal fiber (HCPCF) to SMFs, and cleaving the SMF pigtail to proper length. An interference pattern is formed by the reflected lights from the HCPCF cavity and SMF cavity interfaces. Due to a significant RI difference between these two kinds of fibers, the HCPCF based FPI sensor shows good optical performance, as

* Corresponding author.
E-mail address: jiangmingshun@sdu.edu.cn (M. Jiang).

http://dx.doi.org/10.1016/j.yofte.2016.01.014
1068-5200/

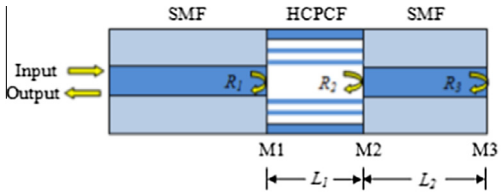

Fig. 1. Structure of the proposed FPI sensor based on HCPCF.

has been confirmed in our previous work [21]. Here we apply this optical fiber FPI biosensor to detecting the growth of yeast (one of the most common microorganism in food production) in liquid culture medium for the first time to the best of our knowledge. During the growth of yeast, the RI changes of analyte can be obtained by measuring the fringe contrast of the sensor interference pattern in real time. The sensor provides a good performance with high resolution and fast response, and shows broad application prospects in biosensing.

2. Theory

Optical fiber FPI based on HCPCF can provide relatively high reflectivity and signal-to-noise ratio, due to the significant RI difference between HCPCF and SMF and the low light transmission loss of HCPCF. Moreover, this kind of FPI sensor is compact and robust. The structure of the proposed FPI sensor is shown in Fig. 1. A short section of HCPCF is performed as an in-fiber air cavity with core RI $n_{HCPCF} \approx 1$. One end of the HCPCF is spliced to SMF, and the other end is spliced to another short section of SMF. The core RI of SMF is different from n_{HCPCH}, thus three reflecting surfaces denoted as M1, M2 and M3 are formed. There are three FP cavities in this structure: Cavity1 formed by M1 and M2 with length L_1, Cavity2 formed by M2 and M3 with length L_2, and the longest Cavity3 formed by M1 and M3 with length equal to $L_1 + L_2$.

The intensity reflectivities of the three surfaces are R_1, R_2 and R_3 respectively, which can be calculated as follows according to the Fresnel reflection equation at normal incidence [19]:

$$R_1 = R_2 = \left[\frac{n_{SMF} - n_{HCPCF}}{n_{SMF} + n_{HCPCF}}\right]^2, \qquad R_3 = \left[\frac{n_{SMF} - n_{EX}}{n_{SMF} + n_{EX}}\right]^2 \tag{1}$$

where n_{SMF} is the core RI of SMF, n_{HCPCH} is the core RI of HCPCF, and n_{EX} is the RI of external medium, i.e., the analyte. When the sensor tip is exposed to air ($n_{EX} = 1$, $n_{SMF} = 1.457$ and $n_{HCPCH} = 1$), R_1, R_2 and R_3 are calculated to be 0.036. With such low reflectivity of each surface, the multiple reflections in the FP cavities can be neglected.

Assume the electric field of the incident light is E_0. The light propagates along the fiber and is reflected by three surfaces respectively. Notice that there is a π phase shift at the surface when light is reflected from an optically denser medium. Here we mainly consider the case of $n_{EX} < n_{SMF}$. Because in most of the biosensing applications, the RI of the samples is typically smaller than 1.37 RIU (refractive index unit) [1,22–24], which is obviously smaller than n_{SMF} (1.457). Thus the combined reflected electric field E_r can be written as the following equation:

$$\begin{aligned} E_r = {} & E_0\sqrt{R_1} + E_0(1-R_1)(1-\alpha_1)(1-\gamma_1)\sqrt{R_2}e^{i(\phi_1+\pi)} \\ & + E_0(1-\alpha_1)(1-\alpha_2)(1-\gamma_1)(1-\gamma_2)(1-R_1) \\ & \times (1-R_2)\sqrt{R_3}e^{i(\phi_1+\phi_2)} n_{EX} < n_{SMF}) \end{aligned} \tag{2}$$

where α_1, α_2 are the intensity attenuation factors due to the mode mismatch and surface imperfection of M1 and M2, respectively; γ_1, γ_2 are defined as the optical transmission loss factors of FP Cavity1 and Cavity2, respectively; Φ_1, Φ_2 are the light phase delays (round-trip) induced by Cavity1 and Cavity2, and can be expressed as:

$$\phi_1 = \frac{4\pi n_{HCPCF} L_1}{\lambda}, \qquad \phi_2 = \frac{4\pi n_{SMF} L_2}{\lambda} \tag{3}$$

where L_1, L_2 are the lengths of Cavity1 and Cavity2 respectively, and λ is the wavelength of incident light.

The normalized intensity reflectivity R_{FP} of the FPI can be calculated by the following equation:

$$R_{FP} = \frac{E_r \cdot E_r^*}{E_0^2} \tag{4}$$

According to Eqs. (1), (2) and (4), the RI of the external medium n_{EX} will affect the output R_{FP} through the intensity reflectivity R_3. Fig. 2 shows the simulated interference spectra (R_{FP} & λ) of the proposed FPI with different n_{EX}. The simulated parameters are: $n_{SMF} = 1.457$, $n_{HCPCH} = 1$, $L_1 = 20$ μm, $L_2 = 775$ μm, $\alpha_1 = \alpha_2 = 0.15$, $\gamma_1 = 0.02$, $\gamma_2 = 0.01$, λ is from 1510 nm to 1590 nm, and $n_{EX} = 1$ (air), 1.315(RI of water at 1550 nm), 1.35 and 1.37, respectively.

As shown in Fig. 2, the fringe contrast of the interference spectrum changes when n_{EX} changes, so the RI of analyte can be determined by measuring the fringe contrast. We choose the fringe that gives the maximum fringe contrast to obtain the highest resolution. By locating the absolute minimum $R_{FP}(\lambda_1)$ and the adjacent peak $R_{FP}(\lambda_2)$ as shown in Fig. 2(b), the maximum fringe contrast can be calculated by $V_{\max} = |10\lg[R_{FP}(\lambda_2)/R_{FP}(\lambda_1)]|$, and in a

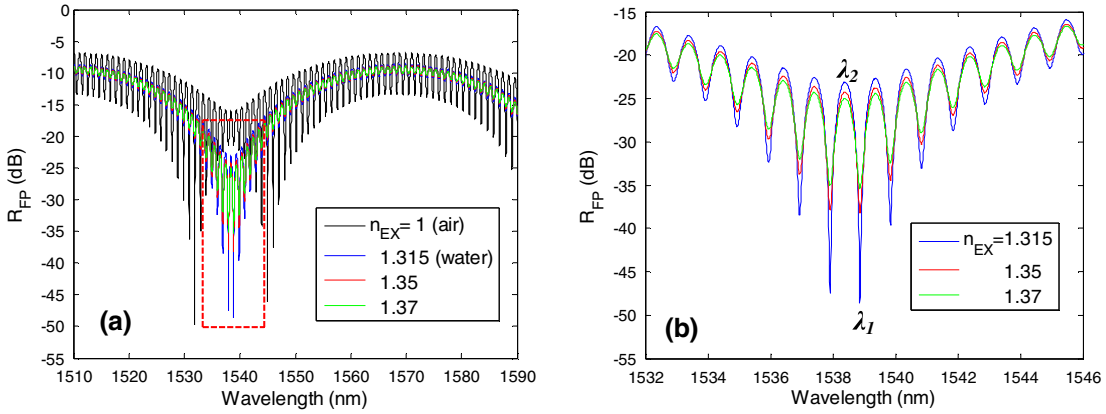

Fig. 2. (a) Simulated interference spectra for $n_{EX} = 1$ (black line), 1.315 (blue line), 1.35 (red line) and 1.37 (green line), respectively (other simulated parameters are: $n_{SMF} = 1.457$, $n_{HCPCF} = 1$, $L_1 = 20$ μm, $L_2 = 775$ μm, $\alpha_1 = \alpha_2 = 0.15$, $\gamma_1 = 0.02$, $\gamma_2 = 0.01$, and λ is from 1510 nm to 1590 nm); (b) close-up of the spectra in solutions of different RI. (For interpretation of the references to color in this figure legend, the reader is referred to the web version of this article.)